Priority Report

Cancer Research

Tomoelastography Distinguishes Noninvasively between Benign and Malignant Liver Lesions

Mehrgan Shahryari[1], Heiko Tzschätzsch[1], Jing Guo[1], Stephan R. Marticorena Garcia[1], Georg Böning[1], Uli Fehrenbach[1], Lisa Stencel[1], Patrick Asbach[1], Bernd Hamm[1], Joseph A. Käs[2], Jürgen Braun[3], Timm Denecke[4], and Ingolf Sack[1]

Abstract

Patients with increased liver stiffness have a higher risk of developing cancer, however, the role of fluid–solid tissue interactions and their contribution to liver tumor malignancy remains elusive. Tomoelastography is a novel imaging method for mapping quantitatively the solid–fluid tissue properties of soft tissues *in vivo*. It provides high resolution and thus has clear clinical applications. In this work we used tomoelastography in 77 participants, with a total of 141 focal liver lesions of different etiologies, to investigate the contributions of tissue stiffness and fluidity to the malignancy of liver tumors. Shear-wave speed (c) as surrogate for tissue stiffness and phase-angle (φ) of the complex shear modulus reflecting tissue fluidity were abnormally high in malignant tumors and allowed them to be distinguished from nontumorous liver tissue with high accuracy [c: AUC = 0.88 with 95% confidence interval (CI) = 0.83–0.94; φ: AUC = 0.95, 95% CI = 0.92–0.98]. Benign focal nodular hyperplasia and hepatocellular adenoma could be distinguished from malignant lesions on the basis of tumor stiffness (AUC = 0.85, 95% CI = 0.72–0.98; sensitivity = 94%, 95% CI = 89–100; and specificity = 85%, 95% CI = 62–100), tumor fluidity (AUC = 0.86, 95% CI = 0.77–0.96; sensitivity = 83%, 95% CI = 72–93; and specificity = 92%, 95% CI = 77–100) and liver stiffness (AUC = 0.84, 95% CI = 0.74–0.94; sensitivity = 72%, 95% CI = 59–83; and specificity = 88%, 95% CI = 69–100), but not on the basis of liver fluidity. Together, hepatic malignancies are characterized by stiff, yet fluid tissue properties, whereas surrounding nontumorous tissue is dominated by solid properties. Tomoelastography can inform noninvasively on the malignancy of suspicious liver lesions by differentiating between benign and malignant lesions with high sensitivity based on stiffness and with high specificity based on fluidity.

Significance: Solid–fluid tissue properties measured by tomoelastography can distinguish malignant from benign masses with high accuracy and provide quantitative noninvasive imaging biomarkers for liver tumors.

Introduction

Liver mechanical properties affect mass formation and treatment outcome (1–3). Specifically, each 1-kilopascal increase in liver stiffness increases the probability of hepatocellular carcinoma (HCC) by 4% (2) and the risk of tumor recurrence after hepatic resection by 16.3% (3). This is the rationale for using elastography to measure mechanical tissue properties of the liver as predictive markers of tumor progression (4).

Complex shear modulus G^* measured by magnetic resonance elastography (MRE) provides a basic description of mechanical tissue properties. Stiffness is usually characterized by magnitude modulus ($|G^*|$), while elasticity and viscosity are quantified by storage (real part of G^*) and loss modulus (imaginary part of G^*), respectively. Phase angle φ of the complex modulus indicates fluidity, equaling zero for pure solids and $\pi/2$ radians (rad) for pure fluids. Thus, fluidity is conceptually signifying the conversion of a solid into a fluid over a continuous range from 0 to $\pi/2$. Materials with $\varphi < \pi/4$ have predominantly solid and materials with $\varphi > \pi/4$ have predominantly fluid properties (5).

Fluidity is currently under investigation as a mechanical property defining the metastatic potential and aggressiveness of tumors (6). Despite many reports on the stiffness of liver tumors (4), little is known about how disease alters the solid–fluid properties of liver tissue. Multifrequency MRE shows that a power-law coefficient related to φ does not change with progression of hepatic fibrosis, while tissue stiffness increases (7). Interestingly, Garteiser and colleagues reported a changed ratio of loss- to-storage properties for liver tumors, suggesting increased fluidity due to carcinogenesis (8). MRE without considering solid–fluid tissue properties is moderately sensitive to malignancy in the liver (8, 9). Given (i) the altered loss modulus in liver tumors (8), (ii) the insensitivity of fluidity to liver fibrosis (7), and (iii) a moderate diagnostic performance of stiffness in identifying liver

[1]Department of Radiology, Charité - Universitätsmedizin Berlin, corporate member of Freie Universität Berlin, Humboldt-Universität zu Berlin, and Berlin Institute of Health, Berlin, Germany. [2]Faculty of Physics and Earth Sciences, Peter Debye Institute, Leipzig University, Leipzig, Germany. [3]Institute of Medical Informatics, Charité - Universitätsmedizin Berlin, corporate member of Freie Universität Berlin, Humboldt-Universität zu Berlin, and Berlin Institute of Health, Berlin, Germany. [4]Department of Diagnostic and Interventional Radiology, University Hospital of Leipzig, Leipzig, Germany.

Note: Supplementary data for this article are available at Cancer Research Online (http://cancerres.aacrjournals.org/).

Corresponding Author: Ingolf Sack, Department of Radiology, Charité - Universitätsmedizin Berlin, Berlin 10117, Germany. Phone: 4930-4505-39058; Fax: 49-30-450-539988; E-mail: ingolf.sack@charite.de

Cancer Res 2019;79:5704–10

doi: 10.1158/0008-5472.CAN-19-2150

tumors (9), we hypothesize that fluidity may be a promising imaging biomarker unaffected by the stiffness of nontumorous liver tissue, which is normally altered by fibrosis. However, fluidity has never been explored in liver tumors; specifically, novel high-resolution multifrequency MRE with tomoelastographic data processing (10, 11) has never been used for this.

Here we use tomoelastography to investigate whether solid–fluid properties can differentiate hepatic tumors from nontumorous liver tissue and malignant from benign lesions. This study was performed to quantify the solid–fluid properties of both tumor and nontumorous liver by tomoelastography.

Patients and Methods

Study design and patients

The study protocol conforms with the Declaration of Helsinki and was approved by the institutional ethics review board (EA1/261/12 and EA1/076/17). All patients gave written informed consent.

From March 2015 to August 2017, the electronic scheduling systems of the departments of liver surgery and radiology were screened for patients with focal liver lesions detected by previous imaging and without contraindications to MRI. Patients with prior treatment of the respective lesion were excluded. The final study cohort included 70 patients with a total of 105 malignant and 36 benign lesions, and 7 healthy volunteers. Diagnoses were 22 HCC, 12 cholangiocarcinoma, 71 metastasis, 11 hemangioma, 10 focal nodular hyperplasia (FNH), and 15 hepatic adenoma. Details are provided in Table 1 and Supplementary Fig. S1.

MRI and MRE

MRI was performed on a 1.5-Tesla Clinical Scanner (Magnetom Aera, Siemens) with a 12-channel phased-array surface coil and the spine-array coils integrated into the table. The MRE sequence and set-up are described in detail elsewhere (11). In brief, mechanical vibrations of 30, 40, 50, and 60 Hz harmonic frequency were induced with two posterior (0.6 bar) and two anterior-pneumatic actuators (0.4 bar) near the liver region (Supplementary Fig. S2). The three-dimensional wave field was acquired by using a single-shot, spin-echo echo-planar imaging sequence with flow-compensated motion-encoding gradients (MEG). Eight phase offsets over a full vibration period were recorded for all three Cartesian-motion field directions. Fifteen consecutive transverse slices with a field-of-view of 384×312 mm^2 (matrix size 128×104) and $3 \times 3 \times 5$ mm^3 resolution were acquired during free breathing. Further imaging parameters: echo time = 59 ms; repetition time = 2,050 ms; parallel imaging with GRAPPA-factor 2; MEG frequency of 43.48 Hz for 30, 40, and 50 Hz vibration frequencies and 44.88 Hz for 60 Hz vibration frequency; and MEG amplitude of 30 mT/m. Total MRE measurement time was approximately 3.5 minutes. More details about the tomoelastography setup are provided in Supplementary Fig. S2.

MRE data processing

MRE data were processed with the tomoelastography pipeline based on multifrequency wavenumber recovery providing maps of shear-wave speed c (in m/s; ref. 10). Because c is deduced

Table 1. Participant characteristics and viscoelastic parameters of tumor and liver

Tumor entities	Participant numbers	Sex female	Age in years (range)	BMI (kg/m^2)	Number of tumors	Tumor diameter in mm (range)	Tumor VOI in cm^3 (IQR)	Tumor c in m/s	Tumor φ in rad	Liver VOI in cm^3 (IQR)	Liver c in m/s	Liver φ in rad
HCC	17	4	67 (43–81)	26.1 ± 3.4	22	30 (12–150)	9.0 (1.7–33.8)	2.54 ± 0.64	1.20 ± 0.29	180 (100–344)	1.97 ± 0.49	0.81 ± 0.16
CCA	10	5	70 (56–76)	25.9 ± 4.1	12	53 (16–124)	11.3 (3.9–164.4)	2.57 ± 0.90	1.24 ± 0.25	252 (156–453)	1.72 ± 0.29	0.66 ± 0.10
MET	27	10	61 (30–85)	25.2 ± 4.0	71	25 (9–175)	5.7 (2.0–12.1)	2.34 ± 0.48	1.14 ± 0.28	210 (104–308)	1.61 ± 0.23	0.65 ± 0.08
HEM	5	5	52 (38–74)	24.0 ± 4.2	11	23 (12–87)	1.8 (1.0–3.6)	1.97 ± 0.45	0.95 ± 0.30	260 (241–329)	1.37 ± 0.13	0.60 ± 0.03
FNH	5	3	38 (29–66)	25.2 ± 5.2	10	21 (9–95)	2.9 (1.5–7.6)	2.08 ± 0.96	0.78 ± 0.24	372 (329–497)	1.40 ± 0.12	0.66 ± 0.04
HCA	8	8	39 (22–52)	25.0 ± 5.0	15	30 (14–90)	5.3 (2.3–22.8)	1.41 ± 0.21	0.66 ± 0.12	226 (143–316)	1.38 ± 0.12	0.66 ± 0.06
Healthy	7	1	35 (28–46)	22.8 ± 3.2	—	—	—	—	—	360 (324–456)	1.39 ± 0.04	0.61 ± 0.03

NOTE: Means are given with ± SD, range or IQR as shown.

Abbreviations: c, shear-wave speed (stiffness); φ, phase angle of the complex shear modulus (fluidity); BMI, body mass index; CCA, cholangiocellular carcinoma; HCA, hepatocellular adenoma; HEM, hemangioma; MET, metastasis; IQR, interquartile range.

from the real part of wave numbers, it can be considered a surrogate of stiffness. Furthermore, we recovered the phase angle of the complex shear modulus, φ (range: 0–π/2). φ > π/4 indicates that loss modulus dominates over storage modulus (12). Both parameters, c and φ, were retrieved by multifrequency dual elasto-visco inversion programs publicly available at https://bioqic-apps.charite.de/downloads. Volumes of interest (VOI), drawn manually, were based on all MRE magnitude images covering tumor or liver and using the information of the lesion's anatomic location obtained by routine MRI. For nontumorous liver tissue VOIs were drawn excluding visible blood vessels.

Statistical analysis

Means were calculated for tumor and liver tissue. Group values were reported as mean ± SD. Different tumor entities in two subjects were considered as independent lesions. Statistical differences between tumor entities were analyzed by the Kruskal–Wallis test. A *post hoc* test with Bonferroni correction for multiple testing was performed. For separation of lesions and nontumorous liver tissue, ROCs were calculated from probabilities predicted by a general linear mixed-effect model (GLMM; ref. 13). The outcome variable was labeled as "liver" or "tumor." We accounted for fixed effects (β) for either c or φ and for nonindependence of multiple tumors within one subject. ROC measures were compared by DeLong method (14).

ROC analysis was performed for characterization (distinguishing malignant from benign lesions). Youden index was calculated to derive optimal cut-off values of φ or c. Sensitivity, specificity, positive predictive value, and negative predictive value were calculated. ROC analysis was repeated without hemangioma because this is easily detected by its strong T2-hyperintensity in MRI (15). Correlation of mechanical properties of tumor and liver was analyzed by Spearman rank correlation coefficient. Statistical analysis was performed in R (version 3.4.3; R-Foundation) using "lme4," "pROC," and "ggplot2" packages. $P < 0.05$ was considered statistically significant. All confidence intervals (CI) stated are for 95%.

Results

Tomoelastography was successful in all participants, that is, there was no drop out due to technical failure. Participant characteristics and group-mean values of c and φ of tumors and liver tissue are summarized in Table 1. MRE maps of four representative cases of malignant lesions including two metastasis, one HCC, and one cholangiocarcinoma are shown in Fig. 1A–D. Figure 2A–D shows four representative cases of benign lesions including two hepatic adenoma, one FNH, and one hemangioma. More cases and additional imaging data are presented in Supplementary Figs. S3A–S3D and S4A and S4B.

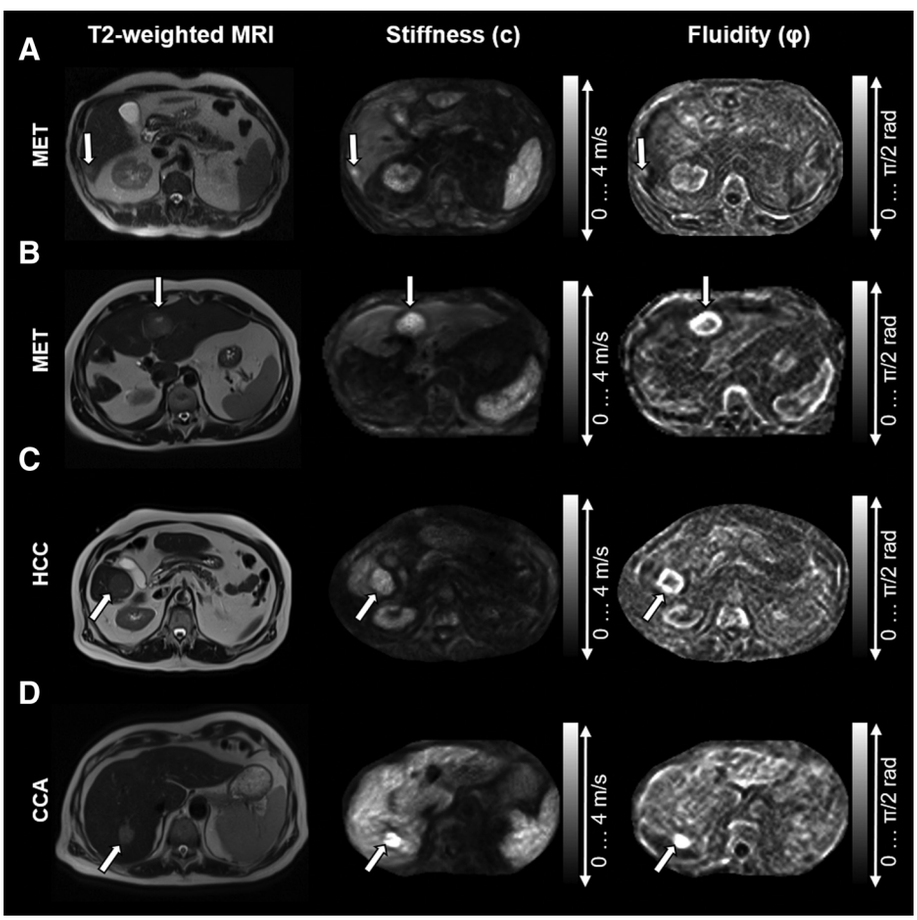

Figure 1.
Tomoelastography results in four representative cases of malignant liver tumors. Shown are maps of shear-wave speed c (stiffness) and phase angle φ (fluidity) along with T2-weighted MR images for anatomic orientation. **A,** Malignant urothelial metastasis (arrow) with 9-mm diameter in a 66-year-old man showing higher c and φ than nontumorous liver tissue. **B,** Fifty-year-old man with hepatic metastasis (MET) of a neuroendocrine tumor (arrow) in the left liver lobe after right hemihepatectomy. The tumor shows high c and φ compared with surrounding liver tissue. **C,** HCC (arrow) in liver segment VI in a 78-year-old man showing high c and φ surrounded by liver tissue stiffened by fibrosis. **D,** Seventy-two-year-old man with a cholangiocarcinoma (CCA; arrow) with larger c than nontumorous liver tissue, although stiffness is increased by fibrosis. φ in cholangiocarcinoma is larger than in nontumorous liver tissue.

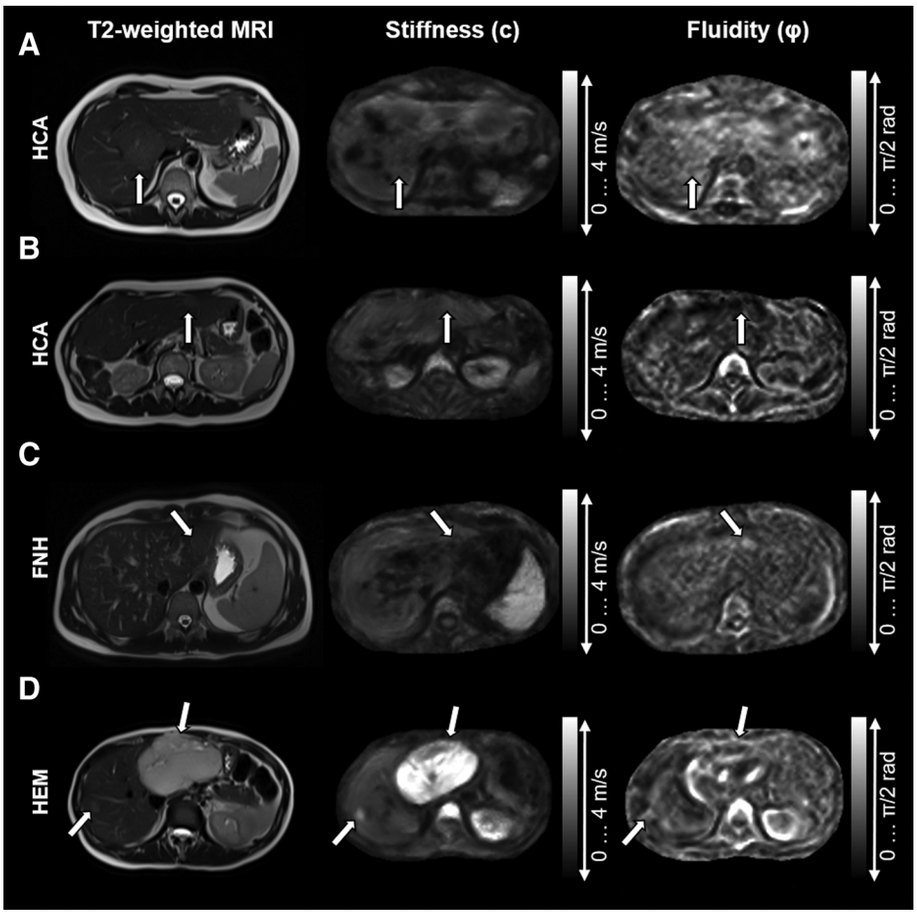

Figure 2.
Tomoelastography results in four representative cases of benign liver tumors. Maps of shear wave speed c (stiffness) and phase angle φ (fluidity) are shown, along with T2-weighted MR images for anatomic orientation. **A,** Benign hepatocellular adenoma (HCA; arrow) in a 40-year-old woman shows similar c and φ to normal, nontumorous liver tissue, making it difficult to separate hepatic adenoma from surrounding liver tissue in tomoelastography maps. **B,** Fifty-two-year-old woman after right partial hepatic resection with hepatic adenoma (arrow), which shows a shear-wave speed and phase angle of the complex shear modulus similar to those in nontumorous liver. **C,** Twenty-two-year-old man with FNH. While FNH (arrow) shows a c similar to that of the surrounding liver, its φ value is slightly above that of the liver. **D,** Two hepatic hemangiomas (HEM) in one slice in a 42-year-old woman. Both hemangioma (arrows) have high T2 signal intensity as well as a high shear-wave speed (c) compared with surrounding liver tissue. Hemangiomas have rather high heterogeneous φ values.

Separation of malignant and benign tumors

Overall, c and φ were significantly larger in malignant lesions (including metastasis, HCC, and cholangiocarcinoma) than in nontumorous liver tissue (respectively, $\beta = 3.62$, 95% CI = 2.41–5.73, $P < 0.001$ and $\beta = 10.64$, 95% CI = 7.02–16.35, $P < 0.001$). GLMM-based ROC analysis showed a significantly larger area under the ROC curve (AUC) of 0.95 (95% CI = 0.92–0.98) for φ, compared with 0.88 (95% CI = 0.83–0.94) for c ($P < 0.01$). Separation of malignant lesions and liver by c was feasible, with a sensitivity of 91% (95% CI = 86–96) and specificity of 70% (95% CI = 59–81), while separation of malignant lesions and liver by φ revealed 92% sensitivity (95% CI = 87–97) and 85% specificity (95% CI = 76–93). Detailed GLMM results for tumor and liver separation based on c and φ are shown in Supplementary Table S1.

Benign lesions (including hemangioma, FNH, and hepatic adenoma) separated from nontumorous liver based on c ($P = 0.03$), while φ was not significantly different ($P = 0.051$). Corresponding AUC values were 0.71 (95% CI = 0.57–0.84) and 0.66 (95% CI = 0.51–0.80) for c and φ, respectively. However, ROC curves of c and φ did not differ statistically ($P = 0.57$).

Results of GLMM-based ROC analysis for separation are shown in Fig. 3A and Supplementary Table S2.

Characterization based on tumor properties

Tumor entities varied significantly in their c and φ properties (both $P < 0.001$). *Post hoc* tests revealed smaller c values for hepatic adenoma than for all malignant tumor entities ($P < 0.001$), but not compared with other benign entities (Fig. 3B). In addition, hepatic adenoma showed smaller φ values than malignant tumors did ($P < 0.01$ vs. HCC and cholangiocarcinoma, $P < 0.001$ vs. metastasis). Two patients with large FNH showed high c and φ values. Additional information can be found in Supplementary Fig. S4A and S4B. Statistical plots of group mean c and φ are shown in Fig. 3B.

A lesion-c threshold of 1.75 m/s allowed distinction between benign and malignant lesions with a very good sensitivity of 94% (95% CI = 87–100) and moderate specificity of 78% (95% CI = 56–94; AUC = 0.85, 95% CI = 0.72–0.98). Similarly, lesion-φ of 0.91 rad, which indicates fluid tissue properties, distinguished benign from malignant lesions with a good sensitivity of 83% (95% CI = 72–93) and moderate specificity of 78% (95% CI = 56–94; AUC = 0.86, 95% CI = 0.77–0.96).

In a total of 13 patients, excluding patients with hemangioma of vascular origin ($n = 5$) from our analysis, diagnostic accuracy increased when the same lesion thresholds of c = 1.75 m/s and φ = 0.91 rad were used. Without hemangioma, sensitivity and specificity of c were very good, at 94% (95% CI = 89–100), and

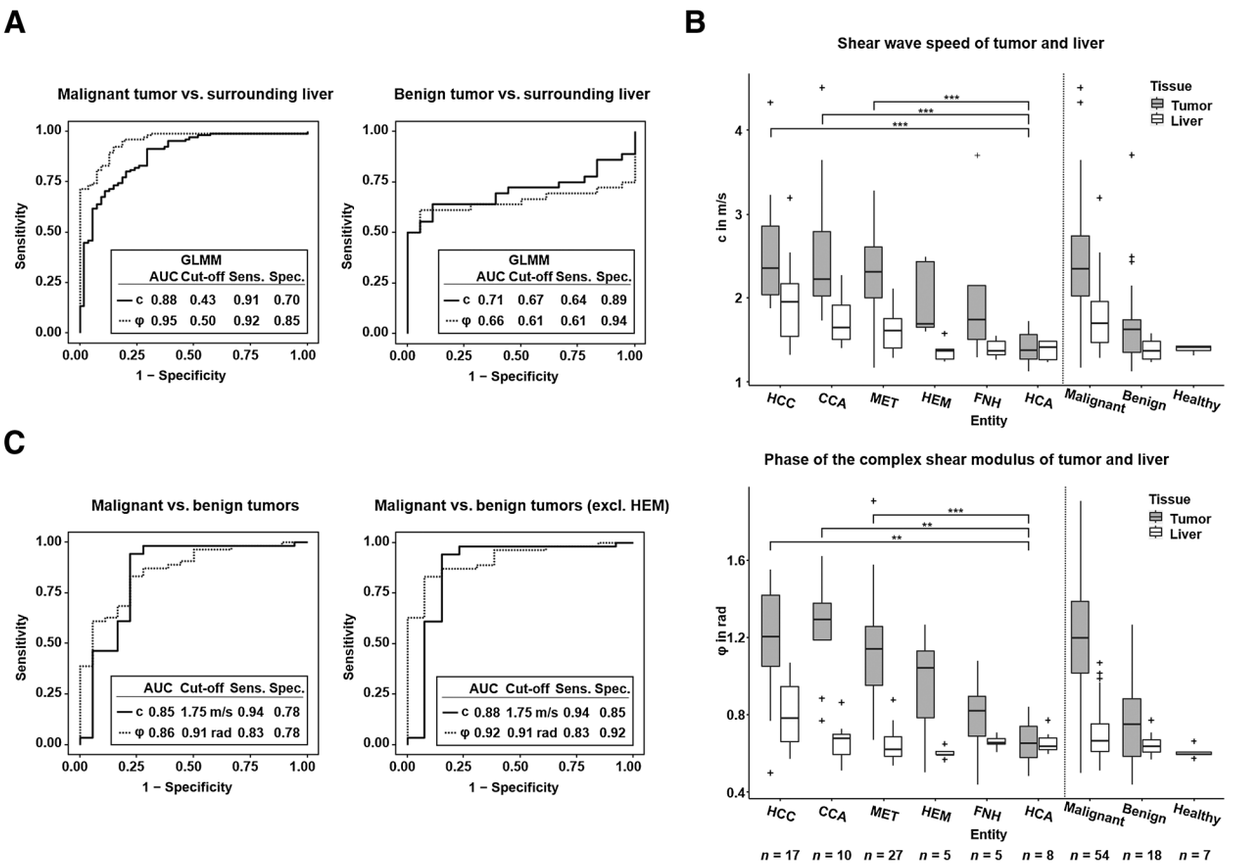

Figure 3.

A, ROC curves based on predictions of GLMM. Left, AUC ROC curve based on model c and φ for separation of malignant lesions and normal liver. Significance for differentiating between the ROC curves was $P < 0.01$ according to DeLong test. Right, ROC based on model c and φ values for separating benign lesions and liver. Here, the two ROC curves are not statistically significantly different ($P = 0.057$). **B,** Boxplot of group shear-wave speed c (top) and fluidity φ (bottom) of tumor and nontumorous liver tissue, for 70 patients and 7 healthy volunteers. *P* values were obtained by the Kruskal–Wallis test, followed by Bonferroni corrected *post hoc* test for comparison between different tumor entities. Bonferroni, *, $P < 0.05$; **, $P < 0.01$; ***, $P < 0.001$. Means and SDs are given in Table 1. **C,** Left, ROC based on tumor-c and tumor-φ for distinguishing patients with malignant from patients with benign tumors. Right, ROC based on tumor-c and tumor-φ for distinguishing malignant and benign tumors, excluding participants with hepatic hemangioma. Detailed information is provided in Supplementary Tables S3 and S4. Sens, sensitivity; spec, specificity.

good, at 85% (95% CI = 62–100; AUC = 0.88, 95% CI = 0.73–1.00), respectively, while those of φ were good, at 83% (95% CI = 72–93) and very good, at 92% (95% CI = 77–100; AUC = 0.88, 95% CI = 0.73–1.00). These results show that diagnostic performance increases when benign tumors of vascular origin are excluded from the characterization of hepatic lesions based on their mechanical properties.

Characterization based on liver properties

We also characterized liver lesions on the basis of nontumorous liver tissue. Liver properties in patients with benign lesions were not different from those of healthy volunteers (all $P > 0.05$). Optimum cutoffs for discrimination of embedded benign tumors from embedded malignant tumors were c = 1.5 m/s and φ = 0.60 rad, the latter being in the range indicating solid tissue properties. Sensitivity and specificity for liver-c were, respectively, moderate, 72% (95% CI = 59–83), and good, at 88% (95% CI = 71–100; AUC = 0.84, 95% CI = 0.75–0.94), while results for liver-φ were poor, at 46% (95% CI = 33–59) and moderate, at 82% (95% CI = 65–100; AUC = 0.60, 95% CI = 0.47–0.73). The inferior diagnostic power of liver-φ compared with tumor-φ indicates noncorrelated fluid properties of liver and embedded lesions. Liver-c of the healthy volunteers showed a stiffness below the cut-off value (1.39 ± 0.04 m/s). Results of ROC analysis for characterization with c and φ are shown in Fig. 3C and Supplementary Table S3.

Liver-c correlated with tumor-c ($P < 0.001$; $r = 0.74$), indicating that tumors preferentially grow in stiff livers, while liver-φ correlated only moderately with tumor-φ ($P < 0.01$; $r = 0.34$) in agreement with the aforementioned insensitivity of liver fluidity to fibrosis.

Discussion

To the best of our knowledge, this is the first study generating fluidity maps for the characterization of liver tumors. We believe that whole-organ tomographic mapping of stiffness

and fluidity with high spatial resolution to depict multiple lesions in the same liver, including lesions smaller than 10 millimeters, is important for quantitative biomechanics-based diagnosis of liver tumors.

Factors contributing to stiffness and fluidity

For further discussion, it is important to note the contributions of elasticity (the tissue's ability to store mechanical energy) and viscosity (its ability to convert mechanical energy into heat) to our parameters. Because c is related to magnitude shear modulus $|G^*|$ by $c^2 = 2 \cdot |G^*| / (\rho \cdot [1 + \cos \varphi])$, it mixes contributions from elasticity and viscosity. Garteiser and colleagues found the loss modulus to be significantly larger in HCCs than in benign hepatocellular tumors, while storage modulus did not differ between these lesion entities (8). Those authors also reported larger $|G^*|$ values for malignant than for benign tumors, probably caused by an increase in loss properties. The sensitivity of the loss modulus to tumor malignancy might be explained by an increase in fluidity due to vascularization or the presence of necrotic tissue. Furthermore, malignant tumors can accumulate hydrophobic, disorganized proteins, which increase tissue stiffness and mechanical friction. This could explain why malignant lesions present as stiff, yet fluid, masses with φ values above the limit of solid–fluid transitions ($\pi/4 = 0.78$ rad). Other mechanisms potentially decrease φ as sketched in Supplementary Fig. S5A–S5C. For example, large organized networks such as portal-to-portal bridges in liver fibrosis or polar water–binding ECM components could reduce φ. In liver fibrosis, the mechanisms that either drive or inhibit fluidity seem to be balanced, rendering the overall fluid–solid behavior of liver tissue insensitive to the progression of fibrosis (7). Similarly, our parameter φ in tumor surrounding liver tissue was not sensitive to malignancy. The apparent insensitivity of φ to liver fibrosis makes fluidity a promising biomechanical marker, with a large difference between tumors and surrounding collagen-rich liver tissues regardless of present fibrosis. Furthermore, in our cohort, abnormal fluidity was specific for malignancy (ruling out solid, benign lesions) while tumor stiffness was sensitive to malignancy (detecting stiff, malignant lesions), thus rendering the combination of the two MRE-based parameters useful for tumor characterization.

Solid–fluid properties in hemangioma

Although fluidity was greater in malignant than benign tumors, we observed high φ values in hemangioma, which can be explained by their vascularity and fluid structure. Vascularity has been reported to increase liver stiffness and viscosity (16). The diagnosis of hemangioma is well established through the European Association for the Study of the Liver guidelines (17). In contrast, hepatic adenoma and FNH can be misinterpreted as malignant tumors when classified by contrast-enhanced MRI alone (18). To address this radiological ambiguity, we performed a second analysis without hemangioma and identified hepatic adenoma and FNH versus malignant masses. In this analysis, overall diagnostic power further increased to 94% sensitivity for c and 92% specificity for φ. It should be noted that in 2 patients with large FNH we observed stiffer and more fluid mechanical properties, similar to those of malignant masses. In those cases, presented in Supplementary Fig. S4A and S4B, hypervascularization due to hyperplastic response to portal tract injury (19, 20) may have been responsible for elevated φ values, while collagen deposition due to scaring could explain higher c values.

Although encouraging, our study has limitations. First of all, by nature of its design, only patients with known liver lesions who needed further diagnostic MRI workup or treatment were enrolled. On the one hand, the distribution of tumor entities in our cohort is typical for a tertiary-care liver center. On the other hand, patient selection is therefore biased toward malignant lesions, as individuals with benign liver tumors (except hepatic adenoma) rarely undergo treatment. For this reason, our study cohort includes a relatively small number of patients with benign liver tumors. Second, not all patients with benign lesions had histopathologic confirmation, but were diagnosed by established imaging criteria in contrast-enhanced MRI. Similarly, not all patients with stiff livers obtained biopsy for confirmation of liver fibrosis or cirrhosis, precluding a correlation analysis of tomoelastography and fibrosis grade. Finally, tomoelastography requires specialized hardware, making set-up and clinical dissemination of the method more difficult than for other innovative MRI methods. Nevertheless, prospective multicenter studies in larger cohorts are planned.

In conclusion, solid–fluid parameters measured by tomoelastography are a promising source of additional diagnostic information in patients with liver tumors including small lesions below 10 mm in diameter. Our results indicate that changes in liver stiffness are related to changes in solid-tissue properties, while changes in tumor stiffness are related to fluid-tissue properties. We propose fluidity as a new imaging marker that holds great promise for tumor detection, irrespective of the stage of liver fibrosis; in conjunction with tissue stiffness, it may allow highly sensitive and specific characterization of liver tumors.

Disclosure of Potential Conflicts of Interest

T. Denecke reports receiving commercial research support and honoraria from Speakers Bureau from Siemens. No potential conflicts of interest were disclosed by the other authors.

Authors' Contributions

Conception and design: M. Shahryari, U. Fehrenbach, T. Denecke, I. Sack
Development of methodology: M. Shahryari, J. Braun, I. Sack
Acquisition of data (provided animals, acquired and managed patients, provided facilities, etc.): M. Shahryari, G. Böning, U. Fehrenbach, T. Denecke
Analysis and interpretation of data (e.g., statistical analysis, biostatistics, computational analysis): M. Shahryari, H. Tzschätzsch, J. Guo, S.R. Marticorena Garcia, P. Asbach, J.A. Käs, I. Sack
Writing, review, and/or revision of the manuscript: M. Shahryari, J. Guo, S.R. Marticorena Garcia, G. Böning, U. Fehrenbach, L. Stencel, P. Asbach, B. Hamm, J. Braun, T. Denecke, I. Sack
Administrative, technical, or material support (i.e., reporting or organizing data, constructing databases): M. Shahryari, S.R. Marticorena Garcia, G. Böning, U. Fehrenbach, L. Stencel, P. Asbach, B. Hamm, J. Braun, T. Denecke, I. Sack
Study supervision: T. Denecke, I. Sack

Acknowledgments

Support of the German Research Foundation (SFB1340 "Matrix in Vision", GRK2260 BIOQIC to I. Sack, J. Braun, J. Guo, P. Asbach, and B. Hamm) and the German Federal Ministry of Education and Research (LiSyM 031L0057 to I. Sack) is gratefully acknowledged.

The costs of publication of this article were defrayed in part by the payment of page charges. This article must therefore be hereby marked *advertisement* in accordance with 18 U.S.C. Section 1734 solely to indicate this fact.

Received July 12, 2019; revised August 31, 2019; accepted September 18, 2019; published first September 24, 2019.

References

1. Ichikawa S, Motosugi U, Enomoto N, Onishi H. Magnetic resonance elastography can predict development of hepatocellular carcinoma with longitudinally acquired two-point data. Eur Radiol 2019;29:1013–21.
2. Singh S, Fujii LL, Murad MH, Wang Z, Asrani SK, Ehman RL, et al. Liver stiffness is associated with risk of decompensation, liver cancer, and death in patients with chronic liver diseases: a systematic review and meta-analysis. Clin Gastroenterol Hepatol 2013;11:1573–84.
3. Wang J, Shan Q, Liu Y, Yang H, Kuang S, He B, et al. 3D MR elastography of hepatocellular carcinomas as a potential biomarker for predicting tumor recurrence. J Magn Reson Imaging 2019;49:719–30.
4. Jiao Y, Dong F, Wang H, Zhang L, Xu J, Zheng J, et al. Shear wave elastography imaging for detecting malignant lesions of the liver: a systematic review and pooled meta-analysis. Med Ultrason 2017;19:16–22.
5. Hirsch S, Braun J, Sack I. Magnetic resonance elastography: physical background and medical applications. Weinheim, Germany: Wiley-VCH; 2017.
6. Koumoutsakos P, Pivkin I, Milde F. The fluid mechanics of cancer and its therapy. Ann Rev Fluid Mechanics 2013;45:325–55.
7. Asbach P, Klatt D, Schlosser B, Biermer M, Muche M, Rieger A, et al. Viscoelasticity-based staging of hepatic fibrosis with multifrequency MR elastography. Radiology 2010;257:80–6.
8. Garteiser P, Doblas S, Daire JL, Wagner M, Leitao H, Vilgrain V, et al. MR elastography of liver tumours: value of viscoelastic properties for tumour characterisation. Eur Radiol 2012;22:2169–77.
9. Venkatesh SK, Yin M, Glockner JF, Takahashi N, Araoz PA, Talwalkar JA, et al. MR elastography of liver tumors: preliminary results. AJR Am J Roentgenol 2008;190:1534–40.
10. Tzschatzsch H, Guo J, Dittmann F, Hirsch S, Barnhill E, Johrens K, et al. Tomoelastography by multifrequency wave number recovery from time-harmonic propagating shear waves. Med Image Anal 2016;30:1–10.
11. Dittmann F, Tzschatzsch H, Hirsch S, Barnhill E, Braun J, Sack I, et al. Tomoelastography of the abdomen: tissue mechanical properties of the liver, spleen, kidney, and pancreas from single MR elastography scans at different hydration states. Magn Reson Med 2017;78:976–83.
12. Hirsch S, Guo J, Reiter R, Papazoglou S, Kroencke T, Braun J, et al. MR elastography of the liver and the spleen using a piezoelectric driver, single-shot wave-field acquisition, and multifrequency dual parameter reconstruction. Magn Reson Med 2014;71:267–77.
13. Liu H, Wu T. Estimating the area under a receiver operating characteristic curve for repeated measures design. J Statistical Software 2003;8:18.
14. DeLong ER, DeLong DM, Clarke-Pearson DL. Comparing the areas under two or more correlated receiver operating characteristic curves: a nonparametric approach. Biometrics 1988;44:837–45.
15. McFarland EG, Mayo-Smith WW, Saini S, Hahn PF, Goldberg MA, Lee MJ. Hepatic hemangiomas and malignant tumors: improved differentiation with heavily T2-weighted conventional spin-echo MR imaging. Radiology 1994;193:43–7.
16. Jamin Y, Boult JK, Li J, Popov S, Garteiser P, Ulloa JL, et al. Exploring the biomechanical properties of brain malignancies and their pathologic determinants in vivo with magnetic resonance elastography. Cancer Res 2015;75:1216–24.
17. European Association for the Study of the Liver (EASL). EASL Clinical Practice Guidelines on the management of benign liver tumours. J Hepatol 2016;65:386–98.
18. Semelka RC, Nimojan N, Chandana S, Ramalho M, Palmer SL, DeMulder D, et al. MRI features of primary rare malignancies of the liver: a report from four university centres. Eur Radiol 2018;28:1529–39.
19. Wanless IR, Mawdsley C, Adams R. On the pathogenesis of focal nodular hyperplasia of the liver. Hepatology 1985;5:1194–200.
20. Nault JC, Bioulac-Sage P, Zucman-Rossi J. Hepatocellular benign tumors-from molecular classification to personalized clinical care. Gastroenterology 2013;144:888–902.